Regimes of local energy pulsations in non-linear Klein-Gordon trimer: Higher dimensional analogs of limiting phase trajectories

V. Kislovsky[1a], M. Kovaleva[2a], Y. Starosvetsky[1]
[1]*Faculty of Mechanical Engineering,*
Technion Israel Institute of Technology,
Technion City, Haifa 32000, Israel

[2]*N. N. Semenov Institute of Chemical Physics,*
Russian Academy of Sciences,
Kosygina st.4 Moscow 119991, Russia

[a] M. Kovaleva and V. Kislovsky contributed equally to this work

ABSTRACT

In the present paper we consider the dynamics of special class of modulated regimes emerging in the Klein-Gordon trimer. In particular, this study unveils the unique states of resonant energy transfer manifested by the regular energy pulsations localized on the first two elements of the chain. This state is regarded as the higher dimensional analog of limiting phase trajectory corresponding to the regime of maximal energy transfer in the 2DOF, anharmonic, oscillatory models. We show that in contrast to the limiting phase trajectories, this special state of local energy transfer emerging in the Klein-Gordon trimer undergoes additional transition leading to its complete elimination. By employing the special order reduction procedure, we describe analytically the mechanism of formation and destruction of this peculiar, dynamical state. Finally, we demonstrate the strong correlation between the bifurcations of this state to the series of spontaneous transitions from localized to delocalized energy pulsations undergone by the impulsive response of the Klein-Gordon trimer. Results of the analytical model are well in agreement with these of the numerical simulations.

1. INTRODUCTION

Over the past decades, nonlinear resonant energy transport and energy localization has been a subject of a rapidly growing interest in various fields of nonlinear physics [1], physics of fluids [2-6], physics of plasma [7], ocean waves [8], semiconductors [9-11]. This well-known phenomenon of resonant energy transport gave rise to many novel ideas for practical applications in various fields of applied physics and engineering [1, 12-17]. Obviously enough, any possible application of the mechanism of nonlinear resonant energy transport to the real-life physical systems requires the substantial theoretical understanding of the intrinsic mechanisms triggering the spontaneous energy flow. Unfortunately, the highly nonstationary nature of this complex, nonlinear phenomenon complicates the development of the analytical predictive capacity which has been proven to be successful only when studying the stationary or weakly nonstationary processes and their bifurcations. The latter has been associated with the well-known concept of nonlinear normal modes (NNMs) [18] broadly applied in the great

variety of physical systems. Importantly, the existing analytical methods which are appropriate for studying the stationary response regimes and NNMs are quite misleading when applied to the classical problems of nonlinear energy transfer emerging in various oscillatory models e.g. coupled anharmonic oscillators, anharmonic oscillatory chains, etc. Recently, the concept of limiting phase trajectories (LPTs) was introduced by Manevitch [19], which is quite natural for a rather comprehensive description of the regime of intense energy transfer - emerging in driven oscillators, coupled generators [20-25], coupled anharmonic oscillators [26 - 29] and oscillatory chains [30-32] as well as the unidirectional energy transport in the oscillatory models with the time varying parameters [33-35].

According to the original definition, LPT corresponds to special regime of two coupled oscillators or, alternatively, an oscillator and an external energy source, manifested by the maximal possible energy transfer. In all the recent studies [20-35] concerning the LPTs authors mainly focused on the resonant interaction of the two coupled fields (e.g. two coupled oscillators, single oscillator driven by the external field, wave-wave interaction in the coupled oscillatory chains, etc.) However, emergence of resonant energy transfer in the dynamical systems admitting the higher dimensional resonance interactions establishes distinct challenges for analytical study and prediction of this highly nonstationary phenomenon.

Analytical predictions of the complex transport phenomena emerging in the short anharmonic chains can be found in some theoretical studies (see e.g. [36,37]) which have analyzed the problem of energy transition to equipartition in short chains in the framework of the classical FPU problem. Another recent study has considered the fundamental problem of the resonant energy transport, emerging in the short FPU chains [31] using the recently developed methodology of limiting phase trajectories.

In the present work we focus on the dynamics of special state of energy transfer emerging in the Klein-Gordon (K-G) trimer which constitutes the higher dimensional analog of the original limiting phase trajectories. This regime is characterized by its spatial localization on the first two elements of the trimer and near complete energy transfer between these elements. To study the global dynamics of this unique regime we use the regular multiscale analysis and derive the slow flow model of the K-G trimer. The evolution of this nonstationary state is further analyzed using the Poincaré maps specially constructed for the slow flow model. We demonstrate that in contrast to the original limiting phase trajectory – its higher dimensional analog undergoes additional transition leading to its complete elimination. Moreover, we show that the well-known mechanism of reconnection of the original limiting phase trajectories (i.e. passing from the moderate to intense energy transport) studied in the 2DOF models is topologically different in the case of the trimer chain. By employing the special, order reduction procedure, we

describe analytically the intricate mechanism of formation and destruction of this unique dynamical state.

2. MODEL AND MOTIVATION

The basic model under consideration is the Klein-Gordon trimer. The nondimensional equations of motion read

$$\begin{aligned}
&\frac{d^2x_1}{dt^2} + x_1 + \varepsilon x_1^{\,3} = \mu\varepsilon\left(x_2 - x_1\right)\\
&\frac{d^2x_2}{dt^2} + x_2 + \varepsilon x_2^{\,3} = \mu\varepsilon\left(x_1 - 2x_2 + x_3\right)\\
&\frac{d^2x_3}{dt^2} + x_3 + \varepsilon x_3^{\,3} = \mu\varepsilon\left(x_2 - x_3\right)
\end{aligned} \qquad (2.1.1)$$

Here x_n - stands for the displacement of n-th oscillator in the trimer, μ is a parameter of coupling, ε is a formal small system parameter scaling the coupling and nonlinear terms. The scheme of the model under consideration is brought in **Figure1.**

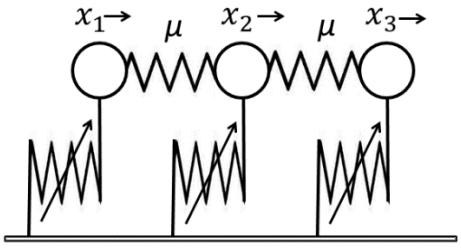

Figure 1. Scheme of the model

The ultimate goal of the present study is to describe the mechanism of emergence and destruction of the special energy transfer state characterized by moderate and intense energy pulsations localized on the first two elements of the K-G trimer. Here we particularly concentrate on the extension of the original LPT concept to the three degrees of freedom system.

3. THEORETICAL STUDY

3.1. Multi-scale analysis and derivation of the slow-flow model

Given the resonant nature of the aforementioned energy transfer state, we anticipate its formation in the neighborhood of the fundamental 1:1:1 resonance. We introduce complex coordinates (C-V) as follows

$$\psi_n = \dot{x}_n + ix_n,\ n = 1,2,3 \qquad (3.1.1)$$

Substituting (3.1.1) into (2.1.1), yields,

$$\psi_1' - i\psi_1 + \frac{\varepsilon i}{8}\left(\psi_1 - \psi_1^*\right)^3 = \frac{i\mu\varepsilon}{2}\left\{\left((\psi_1 - \psi_2) - (\psi_1^* - \psi_2^*)\right)\right\}$$
$$\psi_2' - i\psi_2 + \frac{\varepsilon i}{8}\left(\psi_2 - \psi_2^*\right)^3 = \frac{i\mu\varepsilon}{2}\left\{\left((\psi_2 - \psi_1) - (\psi_2^* - \psi_1^*)\right) + \left((\psi_2 - \psi_3) - (\psi_2^* - \psi_3^*)\right)\right\} \quad (3.1.2)$$
$$\psi_3' - i\psi_3 + \frac{\varepsilon i}{8}\left(\psi_3 - \psi_3^*\right)^3 = \frac{i\mu\varepsilon}{2}\left\{\left((\psi_3 - \psi_2) - (\psi_3^* - \psi_2^*)\right)\right\}$$

The energy transfer state under consideration involves the two characteristic time scales i.e. the scale of fast oscillations (t_0) as well as the scale of slow energy pulsations (t_1) between the coupled oscillators. The competition between the two scales of the dynamic process under consideration is shown on the schematic diagram of Error! Reference source not found.**Figure 2**.

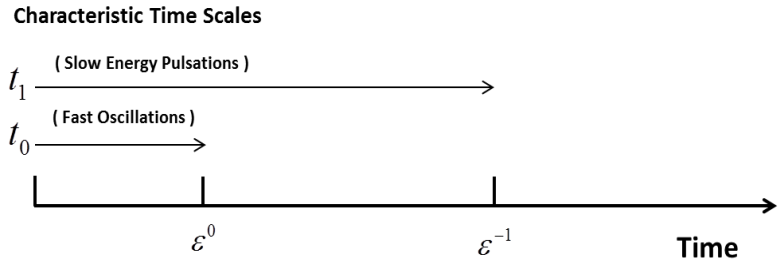

Figure 2. Schematic map of the time scales involved

To analyze the dynamics of (3.1.2) we employ a complex multi-scale expansion

$$\psi_n = \psi_{n0}(t_0, t_1) + \varepsilon\psi_{n1}(t_0, t_1) + O(\varepsilon^2), \frac{\partial(\bullet)}{\partial t} = \frac{\partial(\bullet)}{\partial t_0} + \varepsilon\frac{\partial(\bullet)}{\partial t_1} + O(\varepsilon^2) \quad (3.1.3)$$

Introducing (3.1.3) into (3.1.2) and expanding with respect to the like powers of ε yields at the zeroth order:

$$\dot{\psi}_{n0} - i\psi_{n0} = 0,\ n = 1,2,3 \quad (3.1.4)$$

Solution of (3.1.4) yields,

$$\psi_{n0} = \varphi_n(t_1)\exp(it_0),\ n = 1,2,3 \quad (3.1.5)$$

Proceeding further with the next order of the multi-scale expansion, accounting for (3.1.5) and eliminating the secular terms, read

$$\frac{d\varphi_1}{dt_1} = \frac{3i}{8}|\varphi_1|^2\varphi_1 + \frac{i\mu}{2}(\varphi_1 - \varphi_2)$$
$$\frac{d\varphi_2}{dt_1} = \frac{3i}{8}|\varphi_2|^2\varphi_2 + \frac{i\mu}{2}(\varphi_2 - \varphi_1) + \frac{i\mu}{2}(\varphi_2 - \varphi_3) \quad (3.1.6)$$
$$\frac{d\varphi_3}{dt_1} = \frac{3i}{8}|\varphi_3|^2\varphi_3 + \frac{i\mu}{2}(\varphi_3 - \varphi_2)$$

Before proceeding with the analysis of (3.1.6) we perform additional rescaling $\tau_1 = \frac{3}{8}t_1, \beta = \frac{4\mu}{3}$ yielding the following set of modulation equations in the more simplified form,

$$\begin{aligned}
\frac{d\varphi_1}{d\tau_1} &= i\,|\,\varphi_1\,|^2\,\varphi_1 + i\beta\left(\varphi_1-\varphi_2\right)\\
\frac{d\varphi_2}{d\tau_1} &= i\,|\,\varphi_2\,|^2\,\varphi_2 + i\beta\left(\varphi_2-\varphi_1\right)+i\beta\left(\varphi_2-\varphi_3\right)\\
\frac{d\varphi_3}{d\tau_1} &= i\,|\,\varphi_3\,|^2\,\varphi_3 + i\beta\left(\varphi_3-\varphi_2\right)
\end{aligned} \tag{3.1.7}$$

The system in (3.1.7) possesses two conserved quantities

$$N^2=\sum_{k=1}^{3}|\,\varphi_k\,|^2,\; H=\frac{i}{2}\sum_{k=1}^{3}|\,\varphi_k\,|^4+i\beta\left(\left|\varphi_1-\varphi_2\right|^2+\left|\varphi_2-\varphi_3\right|^2\right) \tag{3.1.8}$$

It is important to note, that without loss of generality we rescale the value of the first conserved quantity N to unity ($N=1$). Using (3.1.8) we introduce the spherical coordinates

$$\begin{cases}
\varphi_1=\cos(\theta)\cos(\varphi)e^{i\delta_1}\\
\varphi_2=\sin(\theta)e^{i\delta_2}\\
\varphi_3=\cos(\theta)\sin(\varphi)e^{i\delta_3}
\end{cases} \tag{3.1.9}$$

Substituting (3.1.9) into (3.1.7) and using the coordinates of the relative phases, i.e. $\Delta_{12}=\delta_1-\delta_2$, $\Delta_{23}=\delta_2-\delta_3$ allows the further reduction of the slow flow system from six to four dimensional sub-space which is spanned by the four angular coordinates. The reduced system, reads

$$\begin{aligned}
\theta' &= \beta\cos(\varphi)\sin(\Delta_{12})-\beta\sin(\varphi)\sin(\Delta_{23})\\
\varphi' &= \beta\tan(\theta)\left(\sin(\Delta_{12})\sin(\varphi)+\sin(\Delta_{23})\cos(\varphi)\right)\\
\Delta_{12}' &= \begin{bmatrix}\cos^2(\theta)\cos^2(\varphi)-\sin^2(\theta)-\beta+\dfrac{\beta}{2}\cot(\theta)\sin(\varphi)\cos(\Delta_{23})\\ -\beta\dfrac{2}{\sin(2\theta)\cos(\varphi)}\left(\sin^2(\theta)-\cos^2(\theta)\cos^2(\varphi)\right)\cos(\Delta_{12})\end{bmatrix}\\
\Delta_{23}' &= \begin{bmatrix}\mathrm{in}^2(\theta)-\cos^2(\theta)\sin^2(\varphi)+\beta-\beta\cot(\theta)\sin(\varphi)\cos(\Delta_{12})\\ -\dfrac{2}{\sin(2\theta)\sin(\varphi)}\left(\cos^2(\theta)\sin^2(\varphi)-\sin^2(\theta)\right)\cos(\Delta_{23})\end{bmatrix}
\end{aligned} \tag{3.1.10}$$

Accordingly the second integral of motion is expressed in terms of the new coordinates ($\theta,\phi,\Delta_{12},\Delta_{23}$):

$$H_{4D}=\begin{bmatrix}\dfrac{i}{2}\left(\left|\sin(\theta)\right|^4+\left|\cos(\theta)\right|^4\left(\left|\cos(\varphi)\right|^4+\left|\sin(\varphi)\right|^4\right)\right)-i\beta\sin(2\theta)\cos(\varphi)\cos(\Delta_{12})\\ -i\beta\sin(2\theta)\sin(\varphi)\cos(\Delta_{23})-i\dfrac{\beta}{2}\cos(2\theta)\end{bmatrix} \tag{3.1.11}$$

In the following section we study the dynamics of locally pulsating regimes exhibited by the reduced slow flow model given by (3.1.10).

3.2. Localized states of resonant energy transfer

3.2.1 Definition of the Extended Limiting Phase Trajectories

Regimes of intense, resonant energy pulsations (strong resonant beats) excited in the 2DOF systems have been broadly considered for the symmetric [19],[24],[27], non-symmetric

[26],[38] as well as the weakly and strongly anharmonic cases [28]. Formation and bifurcations of these highly nonstationary states have been analyzed using the recently developed concept of *limiting phase trajectories* (LPT) [26-28, 44]. In the case of the conservative, two-degrees-of-freedom systems the term limiting phase trajectory corresponds to the unique trajectory of the phase space, **recurrently passing through the strictly localized state of complete energy localization on a single oscillator**. This statement is true for both the symmetric and the asymmetric systems studied in [26-28, 44].

The concept of LPTs provides a useful analytical tool for an adequate description of energy transfer either in the system of two weakly coupled oscillators or in the system of externally driven oscillator [19–35]).

The special type of initial conditions corresponding to the limiting phase trajectory (LPT) emerging in the anharmonic symmetric and asymmetric systems of two coupled oscillators ([19],[26]) have been chosen in a way such that initial excitation (e.g. initial velocity or displacement) is applied solely on the first element of the system. In the same works authors have distinguished between the two types of LPT, i.e. LPT of the first (LPT-I) and the second (LPT-II) kinds. LPT of the first kind corresponds to the permanent energy localization on the first oscillator and weak energy transport between the two, whereas LPT of the second kind corresponds to the intense, recurrent energy transfer between the oscillators. In fact, LPT of the second kind defines the unique regime of **maximal energy exchanges** between the two coupled DOFs.

As we pointed out above the main goal of the present work is to study the mechanism of formation and destruction of the similar regimes of weak and strong energy transfer between the first two elements of the K-G trimer. One of the most interesting properties of the regimes under consideration is their spatial localization on the first two elements of the trimer.

As it will become clear from the results brought below, there is a possible co-existence of several regular (periodic and quasi-periodic) regimes manifested by the moderate and intense, recurrent energy pulsations similarly localized on the first two elements of the trimer model. However, among all the coexisting regimes of the regular, recurrent energy transfer (exhibited by (3.1.10)) one can single out the unique, periodic orbit with the properties similar to the original limiting phase trajectories [26-28,44]. This special periodic orbit can be considered as the higher dimensional analog of LPT and is referred to in the paper as the ***extended limiting phase trajectory (ELPT)***.

We define the ELPT as special orbit of the slow-flow model (3.1.10) satisfying the following properties:

1. Time periodicity – time periodic solution of (3.1.10)

(* We note that the property of time periodicity is defined in accordance with the definition of the original limiting phase trajectory which is a time periodic solution)

2. Spatial localization – Solution of (3.1.10) which is spatially localized on one (the first) or both (the first and the second) elements of the trimer

3. Minimal distance from the strictly localized state – among all the coexisting, periodic solutions satisfying the properties (1) and (2), ELPT has a **minimal distance to the strictly localized state (**i.e. $|\varphi_1| = 1, |\varphi_2| = |\varphi_3| = 0$ or alternatively ($\theta = \phi = 0$ **),** complete energy localization on the first element).

(** We note that this property is dictated by the definition of the original limiting phase trajectory (see e.g. [19], [26-28], [38]), which has been defined as a unique, periodic orbit which recurrently passes through the strictly localized state i.e. state of complete energy localization on the first (initially excited) element.)

In the context of the considered 3DoF system (K-G trimer), ELPT can be viewed as a three dimensional analog of the non-symmetric LPT analyzed in [26], [38]. Similarly to the previous results concerning the original limiting phase trajectories the extended ones can also be distinguished by the form of energy localization and intensity of energy transport between the two elements of the chain:

ELPT of the **First Kind** (**ELPT-I**) corresponds to the **significant energy localization on the first element** and **moderate energy transport** between the first and the second elements of the chain.

ELPT of the **Second Kind** (**ELPT-II**) corresponds to the **spatial energy localization on the first two elements of the chain**, accompanied with the **intense energy transport** between them. In fact, ELPT-II possesses an additional (fourth) property of immense importance.

4. Maximal Energy Transfer - among all the coexisting, periodic solutions satisfying the properties (1) and (2) – ELPT of the second kind corresponds to the special energy transfer state characterized by the maximal amount of energy exchange between the first and the second elements of the trimer. (*** We note that the last property of extreme energy transport is defined in accordance with the definition of the original limiting phase trajectory of the second kind (LPT-II) which defines the unique regime of **maximal energy exchange** between the two coupled DOFs.)

As it will become evident from the results below, system under consideration (3.1.10) can also maintain the other types of periodic solutions satisfying the first and the second properties but not the last two.

3.2.2 Evolution of the Extended Limiting Phase Trajectories

In the present section we study the global evolution of the extended limiting phase trajectories (ELPTs) along with the variation of the system parameters. To this end we resort to the construction of Poincaré maps for the slow-flow model (3.1.10). Obviously enough, the global

dynamics of (3.1.10) is too complicated to be amenable by a straightforward analytical treatment. However, it is still possible to study the intrinsic mechanism of formation and destruction of the ELPT by constructing Poincaré maps for the slow flow system (3.1.10) at the fixed energy levels. Accordingly we fix the value of the Hamiltonian H (given in (3.1.11)) to some constant, thus restricting the flow of (3.1.10) to a three-dimensional iso-energetic manifold,

$$H(\theta, \phi, \Delta_{12}, \Delta_{23}; \beta) = h \tag{3.1.12}$$

By transversely intersecting the three-dimensional iso-energetic manifold by the cut plane $T: \{\theta = \theta_0\}$ we construct the two dimensional Poincaré map $P: \boldsymbol{\Sigma} \to \boldsymbol{\Sigma}$, which is defined as

$$\boldsymbol{\Sigma} = \{\theta = \theta_0,\ \theta' < 0\} \cap \{H(\theta, \phi, \Delta_{12}, \Delta_{23}) = h\} \tag{3.1.13}$$

The restriction $\theta' < 0$ is intentionally imposed to make the constructed Poincaré map an orientation preserving. The fundamental time-periodic solutions of a basic period T correspond to the period-1 fixed points of the Poincaré map, i.e., periodic orbits of system (3.1.10) that recurrently pierce the cut section at a single point. Additional subharmonic solutions of periods nT may exist corresponding to period-n equilibrium points of Poincaré map, i.e., to orbits that pierce the cut section n times before repeating themselves. In the present study we construct the Poincaré map $P: \boldsymbol{\Sigma} \to \boldsymbol{\Sigma}$ such that the global flow defined by (3.1.10) is mapped onto the (Δ_{12}, ϕ) plane.

As it was pointed out in the previous subsection, apart from ELPT there exist additional *periodic orbits* (**PO**) of (3.1.10). These additional periodic solutions can be classified in accordance with the form of their localization. Here we define the three types of periodic orbits of (3.1.10) emerging as the 1-period fixed points of the Poincaré maps discussed below.

1. Localized Periodic Orbit 100 – time-periodic orbit with spatial localization on the first element**.**

2. Localized Periodic Orbit 110 – time-periodic orbit with spatial localization on the first two elements.

3. Periodic Orbit (**PO)** – delocalized time-periodic orbit.

These three distinct types of periodic orbits are denoted in the Poincaré sections as **LPO {1,0,0}, LPO {1,1,0}** and **PO**, accordingly. According to the new definition of a general class of the time periodic orbits – ELPT-I falls under the category of LPO {1,0,0} type orbits, while ELPT-II falls under the category of LPO {1,1,0}. Here we classified only few of the periodic solution relevant to the evolution of ELPT. The detailed classification of the entire family of periodic orbits of the slow flow model deserves a separate study and will be published elsewhere.

As a next step we will further investigate the evolution of ELPT on the Poincaré sections along with the variation of the system parameters. Given the third property of ELPT it is convenient to study its evolution on the iso-energetic manifold corresponding to the strictly localized state

($\theta = \phi = 0$). This restriction immediately defines the following constant for the Hamiltonian (3.1.11),

$$h(\beta) = \frac{i}{2}(1-\beta) \tag{3.1.14}$$

The Poincaré sections illustrated in **Figure 3** (a-d) correspond to the different values of coupling parameter β. In scope of the present study we focus solely on the evolution of **ELPT**. Let us start the discussion from the Poincaré section of **Figure 3a** corresponding to the lower value of coupling.

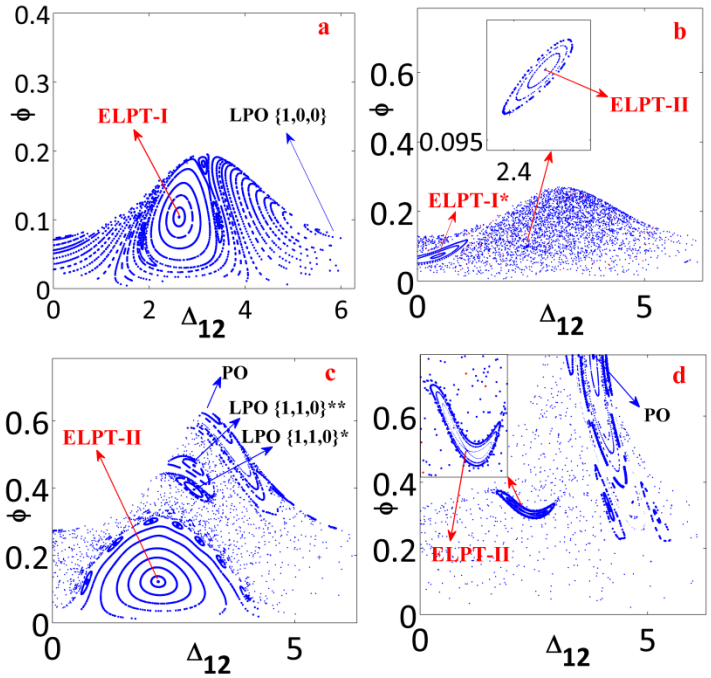

Figure 3. Poincaré sections ($\theta_0 = 0.34$): (a) $\beta = 0.15$; (b) $\beta = 0.17101$; (c) $\beta = 0.28$; (d) $\beta = 0.364$.

Poincaré section of **Figure 3a** unveils two period-1 orbits. As is shown in **Figure 3a**, one of the orbits corresponds to the **ELPT-I** whereas the second periodic orbit is an **LPO** with the spatial energy localization on the first element (**LPO {1,0,0}**). The time histories of these periodic orbits are shown in **Figure 5(a, b)**. Observation of these two plots - clearly shows that the second LPO is more distant from the localized state (**$\theta(\tau_1) = \phi(\tau_1) = 0$**) than the **ELPT-I** (as it is required by the third property of the previous section).

Along with the periodic solutions of the Poincaré section it is essential to discuss the special family of the quasi-periodic orbits encircling the (ELPT-I) period-1 fixed points. These quasi-periodic solutions encircling the ELPT-I center possess the similar properties of strong energy localization on the first element and weak quasi-periodic energy pulsations. It is thus rather natural to attribute this special class of quasi-periodic orbits to the same regular state of the weak local energy pulsations. To examine the further evolution of ELPT, we increase the value of the coupling strength. The corresponding Poincaré section is illustrated in **Figure 3b**. Results

of **Figure 3b** clearly show the coexistence of two period-1 fixed points (centers). The first center corresponds to the previously observed ELPT-I whereas the second center corresponds to the newborn orbit ELPT-II. The latter is formed through the typical (saddle – center) bifurcation. The time histories corresponding to the (ELPT-II) and these of (ELPT-I*) are shown in **Figure 5** (c, d), correspondingly.

Interestingly enough, **the mechanism of formation of the ELPT-II in the considered 3DOF model qualitatively differs from the results reported for the 2DOF models** [26], [38]. Indeed, as it was reported in [26-28], [38], the mechanism of formation of the LPT of the second kind in the 2DOF models is through its typical reconnection with the LPT of the first kind, bringing to the complete elimination of the latter. However, as we observe for the 3DOF case – formation of ELPT-II does not bring to the elimination of ELPT-I and there is a short overlapping region of both orbits (i.e. $\beta = \beta^1_{ELPT} \approx 0.17101$ - formation of the ELPT-II, $\beta = \beta^* \approx 0.1991$ - destruction of the ELPT-I).

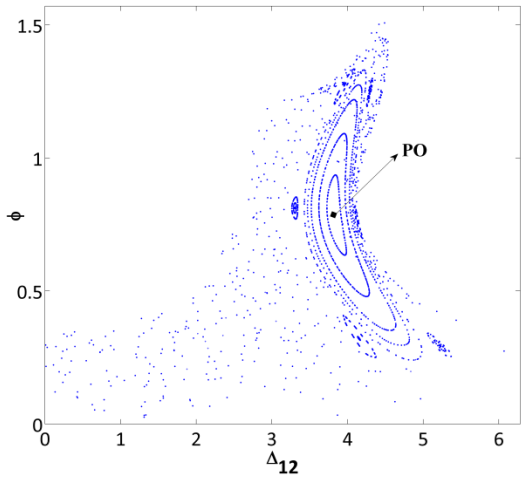

Figure 4. Poincaré section ($\theta_0 = 0.34$), $\beta = 0.37$

It is important to point out that according to the above definition ELPT is defined as a unique solution. Thus, examining the third property of both coexisting orbits (ELPT-I and -II) we found out that the newly formed periodic solution (ELPT-II) has a minimal distance to the strictly localized state (this observation can be also inferred from the time histories shown in **Figure 5** (c, d)). It also means that in the overlapping region - ELPT-I cannot be regarded as ELPT orbit and is denoted in **Figures 3b** and **5d** as ELPT-I*. Thus according to the above definition the new formed orbit (ELPT-II) constitutes the unique *extended limiting phase trajectory* of the second kind. Formation of ELPT-II has been recorded for ($\beta = \beta^1_{ELPT} \approx 0.17101$). **In what follows we solely concentrate on the mechanisms of formation and destruction of ELPT-II.**

Arguing as above we note once again that the quasi-periodic solutions encircling the ELPT-II center possess the similar properties of energy localization on the first two elements of the chain and intense, quasi-periodic energy pulsations. It is thus rather natural to attribute this special class of quasi-periodic orbits to the same regular state of the intense local energy pulsations. Formation of this new regular state is further referred to as the first transition undergone by ELPT.

To examine the further evolution of the ELPT we construct the additional Poincaré section (**Figure** 3c) for the significantly increased value of coupling ($\beta = \beta_{ELPT}^{1} \approx 0.28$). This section reveals four period-1 orbits. Three out of four periodic orbits belong to the LPO {1,1,0} while the fourth orbit is a delocalized orbit which does not fall under category of LPO {1,0,0} and LPO {1,1,0} orbits. As it is apparent from the previous discussion, among all the localized, periodic solutions of type (LPO {1,1,0}) there is a unique orbit admitting the definition of the extended limiting phase trajectory (see **Figure 3c**). To draw the comparison between the ELPT-II and other (LPO) orbits of the section (corresponding to $\beta = 0.28$) we plot their time histories in **Figure 6(a, b, c)**. As is evident from the results of **Figure 6(a, b, c)**, among the three LPO orbits - ELPT-II shows the highest amount of energy transport (per one oscillation cycle) between the first and the second elements and has the minimal distance from the strictly localized state.

Further inspection of the evolution of the Poincaré section with respect to the growing value of the coupling strength (β) shows the gradual destruction of the resonance islands corresponding to all the LPO {1,1,0} – type orbits (including ELPT-II). In the Poincaré section of **Figure 3d** one can easily observe the annihilation of almost all resonant islands corresponding to the LPOs {1,1,0} besides the one of ELPT-II. Moreover, as it can be inferred from the results of **Figure 3d**, ELPT-II undergoes the period-doubling bifurcation (PD). The time histories corresponding to the periodic orbit with the doubled-period is illustrated in **Figure 6d** and is denoted as **ELPT-II (PD)**.

Further increase in the strength of coupling i.e. $(\beta = 0.37)$ shows the vanishing of all the resonant islands corresponding the LPO{1,1,0} type orbits. This can be clearly seen from the results of the Poincaré section of **Figure 4**. Evidently enough, the resonant island containing the ELPT-II is the "last surviving", regular state of energy transport localized on the first two elements of the trimer. In the present study we refer to the destruction of this regular state as the second transition occurring at ($\beta_{ELPT}^{2} \approx 0.37$).

In **Table** 1 we summarize the transition values for the ELPT. In the following section we devise the analytical procedure based on the construction of the reduced order model predicting all the aforementioned transitions undergone by ELPTs.

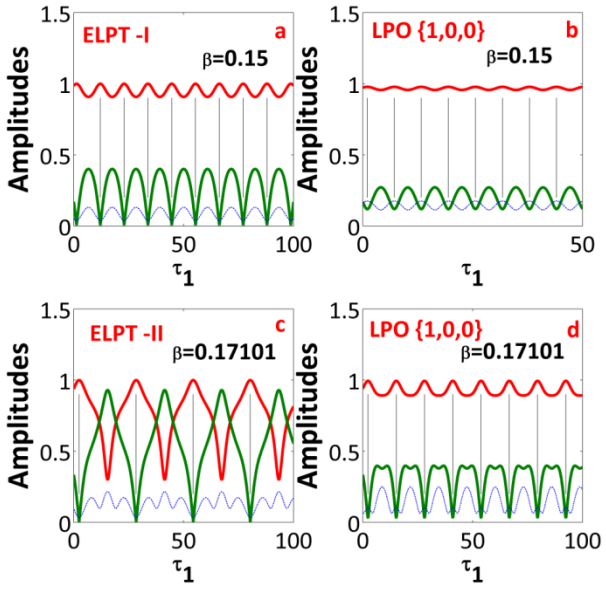

Figure 5. Time histories of the amplitudes of the periodic orbits ($|\varphi_1|,|\varphi_2|,|\varphi_3|$) (a) ELPT-I ($\beta = 0.15$); (b) LPO {1,0,0} ($\beta = 0.15$); (c) ELPT-II ($\beta = 0.17101$); (d) LPO {1,0,0} ($\beta = 0.17101$). Amplitudes $|\varphi_1|,|\varphi_2|,|\varphi_3|$ are plotted in bold solid red, bold solid green and dash-dot thin blue lines, respectively.

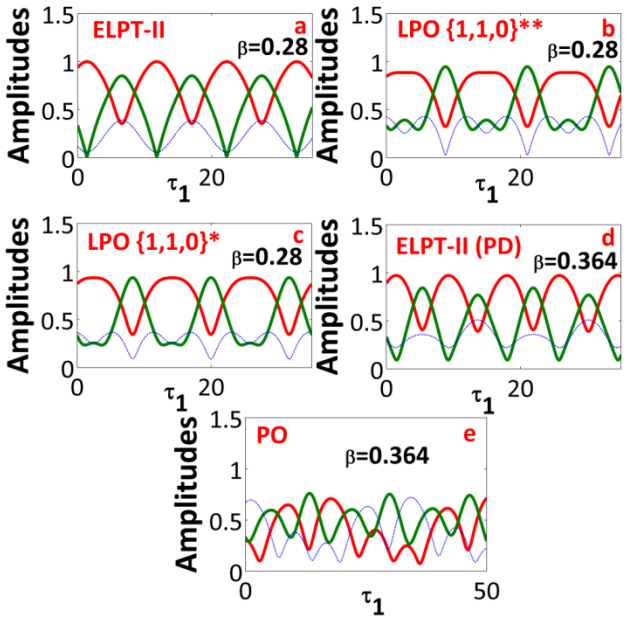

Figure 6. Time histories of the amplitudes of the periodic orbits ($|\varphi_1|,|\varphi_2|,|\varphi_3|$) (a) ELPT {1,1,0} ($\beta = 0.28$); (b) LPO {1,1,0} ($\beta = 0.28$, marked as LPO** in Figure 3c); (c) LPO {1,1,0} ($\beta = 0.28$, marked as LPO* in Figure 3c); (d) ELPT-II ($\beta = 0.364$); (e) PO ($\beta = 0.364$). Amplitudes $|\varphi_1|,|\varphi_2|,|\varphi_3|$ are plotted in bold solid red, bold solid green and dash-dot thin blue lines, respectively.

	1st Transition	**2nd Transition**
ELPT-II (Poincaré sections)	$\beta^1_{ELPT} \approx 0.17101$ (Formation of ELPT-II)	$\beta^2_{ELPT} \approx 0.37$ (Destruction of ELPT-II)

Table 1. Transition values for ELPT

We note that numerical integration procedure of (3.1.10) used for the construction of Poincaré sections of the present subsection have been performed in Matlab using the ODE45 solver with the scalar relative error tolerance of 1×10^{-8} and a vector of absolute error tolerances AbsTol of 1×10^{-8}. The algorithm of ODE45 is based on an explicit Runge-Kutta (4,5) formula, the Dormand-Prince pair. It is also important to point out that in chaotic regions of the Poincaré sections it is rather hard to avoid the extra chaotic effects generated by the numerical solver due to the extreme sensitivity of the system to the initial conditions (in these regions). However in scope of the present work we mainly focus on the regular dynamics of (3.1.10). Zones of regular regimes have been reproduced on the Poincaré maps and no overlap with the chaotic regions has been observed.

3.2.3 Analytical prediction of the zone of existence of strong, local energy pulsations (ELPT-II)

In the present subsection we construct the simplified analytical model predicting the first and the second transitions undergone by ELPT-II defining the important zone of existence of the intermediate transport states of regular, localized, intense energy pulsations. As we have already emphasized above, the ELPTs can be viewed as a higher dimensional analogs of the, non-symmetric limiting phase trajectories emerging in the 2DOF systems [26], [38]. Motivated by this observation we are willing to apply the existing methodology of the limiting phase trajectories on the 3DOF system under consideration. To this extent we make the following assumption:

For both kinds of ELPTs (i.e. I and II) we assume that the response on the third element of the chain is negligibly small (in comparison to the first and the second elements) i.e. $|\varphi_1| >> |\varphi_3|, |\varphi_2| >> |\varphi_3|$ (where $|\varphi_1|, |\varphi_2| \square O(1)$)

Based on this assumption one can simplify the slow –flow model (3.1.10) by employing the idea of a 'master and slave' decomposition. To this end we approximate the response of the first two elements described by (3.1.7) with the reduced (approximate) 2DOF model by setting the amplitude of the response of the third element to zero in the first two equations of (3.1.7). This yields the following, non-symmetric 2DOF system.

$$\begin{aligned} \varphi_1' &= i\varphi_1|\varphi_1|^2 + i\beta(\varphi_1 - \varphi_2) \\ \varphi_2' &= i\varphi_2|\varphi_2|^2 + i\beta(2\varphi_2 - \varphi_1) \end{aligned} \tag{3.1.15}$$

Proceeding along these lines, we simplify the third equation of (3.1.7) by neglecting the nonlinear term (due to the smallness of $|\varphi_3| << 1$) and retain solely the terms containing $\varphi_2(\tau_1)$ as an external field exciting the third element

$$\varphi_3' = i\beta\varphi_2 \tag{3.1.16}$$

Thus, application of the master and slave decomposition on the slow-flow model yields the two decoupled systems. The first system (3.1.15) depicts the dynamics of the free response of the first two coupled elements, while the second system (3.1.16) depicts the dynamics of the third element being excited by the response of the central element of the chain. In the following two subsections we use the decomposed system (3.1.15) and (3.1.16) to predict the formation and destruction of ELPT-II.

3.2.3.1 Analytical estimates of the formation of ELPT-II

To construct the analytical estimate for the numerically obtained critical value of the coupling strength (β) corresponding to the formation of ELPT-II (β_{ELPT}^{1}) we resort to the (2DOF) theory of LPTs which has been recently applied on the planar non-symmetric anharmonic systems [26], [38]. Before proceeding with the analysis let us briefly sketch the idea of the approximation. Recalling that both ELPT-I and ELPT-II correspond to the significant energy localization on the first two elements of the trimer (i.e. $|\varphi_1| >> |\varphi_3|, |\varphi_2| >> |\varphi_3|$), thus formation of the ELPT-II can be associated with the well-known, global bifurcation ('reconnection') undergone by the limiting phase trajectories in the approximate, reduced order model (3.1.15) (see e.g. [26],[27],[38]). Thus, the critical value of $\beta = \beta_{LPT}^{1}$ corresponding to the point of 'reconnection' undergone by the LPT in the 2DOF model (3.1.15) will constitute the crude, asymptotic estimate for the critical value (β_{ELPT}^{1}) of the full model (3.1.10).

The system (3.1.15) exactly falls under the category of the anharmonic system considered in [26], [38]. For the sake of clarity we briefly repeat the analysis developed in [26]. Obviously the system in (3.1.15) is integrable and possesses the two integrals of motion, namely the Hamiltonian

$$H = \frac{i}{2}\left(|\varphi_1|^4 + |\varphi_2|^4\right) + i\beta|\varphi_1 - \varphi_2|^2 + i\beta|\varphi_2|^2 \tag{3.1.17}$$

and the occupation number,

$$N = |\varphi_1|^2 + |\varphi_2|^2 \tag{3.1.18}$$

Arguing exactly as above we set N to unity ($N = 1$) and introduce the angular coordinates,

$$\varphi_1(\tau) = \cos(\theta)e^{i\delta_1},\ \varphi_2(\tau) = \sin(\theta)e^{i\delta_2},\ \Delta = \delta_1 - \delta_2 \tag{3.1.19}$$

Here the angular amplitude θ also stands for the energy distribution between the coupled elements, $\delta_i\,(i = 1,2)$ is the absolute phase of the response of i-th element, while Δ is the relative phase. Substituting (3.1.19) into (3.1.15) yields the following planar system described in terms of the angular coordinates,

$$\theta' = \beta \sin(\Delta)$$
$$\sin(2\theta)\Delta' = \frac{1}{2}\sin(4\theta) + 2\beta\cos(\Delta)\cos(2\theta) - \beta\sin(2\theta) \tag{3.1.20}$$

The system's Hamiltonian given in (3.1.17) can be represented in the following angular form,

$$H = \frac{i}{2}\left(\sin^4(\theta) + \cos^4(\theta)\right) - i\beta\sin(2\theta)\cos(\Delta) + i\beta\sin^2(\theta) \tag{3.1.21}$$

We proceed with finding the fixed points of (3.1.20). As is clear from the recent works (considering the theory of LPT), the fixed points of (3.1.20) play a crucial role in the global system dynamics. Apparently, fixed points of (3.1.20) admit the following set of algebraic equations (by setting the time derivatives of (3.1.20) to zero),

$$\frac{1}{4}\sin(4\theta) + \beta\cos(2\theta) - \frac{\beta}{2}\sin(2\theta) = 0,\ \Delta = 0 \tag{3.1.22}$$

$$\frac{1}{4}\sin(4\theta) - \beta\cos(2\theta) - \frac{\beta}{2}\sin(2\theta) = 0,\ \Delta = \pi \tag{3.1.23}$$

Obviously enough, solutions of (3.1.22) correspond to the in-phase nonlinear normal modes, whereas solutions of (3.1.23) correspond to the out-of-phase ones. To find all the solutions of (3.1.22) and (3.1.23) explicitly is beyond the scope of the current paper. In **Figure 7** we illustrate the three phase portraits of the planar system (3.1.20) for the three distinct values of the coupling strength β. In terms of the slow-flow model (3.1.20), the regime of intense energy transport between the oscillators corresponds to a special orbit that passes through the state $\theta = 0$ and reaches the vicinity of $\theta = \frac{\pi}{2}$. As can be easily deduced from (3.1.19), these two conditions ensure a nearly complete energy exchange between the oscillators. This special type of trajectory is referred to in the literature as a limiting phase trajectory of the second kind [26], [38].

In **Figure 7a** one can clearly see the existence of a special orbit containing the branch of $\theta(\tau_1) = 0$. This trajectory is denoted with a bold solid line. Apparently this orbit does not correspond to the intense energy transport between the oscillators as it stays away from $\theta = \pi/2$ (which is a necessary condition for the significant energy transport to the second oscillator). We refer to this type of trajectory as the **LPT of the first kind**. This unique trajectory is characterized by the significant energy localization on the first element and moderate energy transport between the oscillators (see **Figure 8a**).

Increasing the value of β up to a certain critical value ($\beta = \beta_{LPT}^1$), one observes a coalescence of the LPT of the first kind with a separatrix of a saddle point ($\theta = \theta_{saddle}, \Delta = \pi$) which is given by the solution of (3.1.23) (see **Figure 7c**). This coalescence of the LPT with the separatrix leads to the reconnection between the branches of LPT giving rise to the formation of the **LPT of the second kind** (see **Figure 7b**).

As is clear from the discussion of the previous subsection, these regular LPT orbits constitute the lower dimensional analogs of ELPTs. Namely, there are clear similarities between the

ELPT-I and -II orbits and the LPTs of the first (LPT-I) and second (LPT-II) kind, respectively. For instance, similarly to the ELPT-I the LPT-I is localized on the first element and is manifested by the moderate energy pulsations. In the same manner, ELPT-II is similar to the regular LPT-II orbit as it exhibits the intense energy pulsations between the first two elements of the trimer. Moreover, both LPT and ELPT admit the property of having the minimal distance from the strictly localized state.

To illustrate this similarity between these two unique solutions we plot the time histories for the amplitudes of $|\varphi_1(\tau_1)|,|\varphi_2(\tau_1)|$ (for the same value of the coupling parameter) corresponding to LPT of the reduce model (3.1.15) (**Figure 8a**, **8**c) and ELPT of the trimer (3.1.7) (**Figure 8b, 8d**) of both kinds. From the results of **Figure 8** one can infer the striking similarity of these special orbits of the reduced and the full models. As we have already noted above, the main goal of the analysis of the simplified model (3.1.20) is the derivation of the analytical estimate for (β^1_{ELPT}) corresponding to the numerically observed formation of ELPT-II in the trimer model. To this end we look for the special value of β corresponding to the 'reconnection' of the limiting phase trajectory in the approximate, simplified system(3.1.20). Following the results reported in [26], [38], we note once again that the limiting phase trajectory of (3.1.20), is uniquely defined as a special trajectory containing the branch of $\theta(\tau_1)=0$. As was shown in the same works, the analytical criterion for the derivation of the first, critical, value of coupling corresponding to the reconnection of LPT can be deduced directly from the Hamiltonian (3.1.21). Thus, LPT trajectory is implicitly defined by the Hamiltonian (3.1.21) as

$$\left(\sin^4\left(\theta_{LPT}\right)+\cos^4\left(\theta_{LPT}\right)\right)-2\beta\sin\left(2\theta_{LPT}\right)\cos\left(\Delta_{LPT}\right)+2\beta\sin^2\left(\theta_{LPT}\right)=1 \qquad (3.1.24)$$

As we pointed out above - the reconnection of the LPT of the first kind with that of the second kind occurs for the special value of coupling $\beta=\beta^1_{LPT}$ where the LPT trajectory passes through the saddle point ($\theta=\theta_{saddle},\Delta=\pi$) given by (3.1.23). Unfortunately, exact solution of (3.1.23) is a formidable task and therefore we formulate the analytical criterion for the coupling threshold $\beta=\beta^1_{LPT}$ implicitly. Thus the critical value β^1_{LPT} and the corresponding value of the θ_{saddle} can be found from the simultaneous solution of the following set of trigonometric equations,

$$\begin{aligned}&\left(\sin^4\left(\theta_{saddle}\right)+\cos^4\left(\theta_{saddle}\right)\right)+2\beta^1_{LPT}\sin\left(2\theta_{saddle}\right)+2\beta^1_{LPT}\sin^2\left(\theta_{saddle}\right)=1\\&\frac{1}{4}\sin\left(4\theta_{saddle}\right)-\beta^1_{LPT}\cos\left(2\theta_{saddle}\right)-\frac{\beta^1_{LPT}}{2}\sin\left(2\theta_{saddle}\right)=0\end{aligned} \qquad (3.1.25)$$

Solution of (3.1.25) yields $\beta^1_{LPT}=0.1741$.

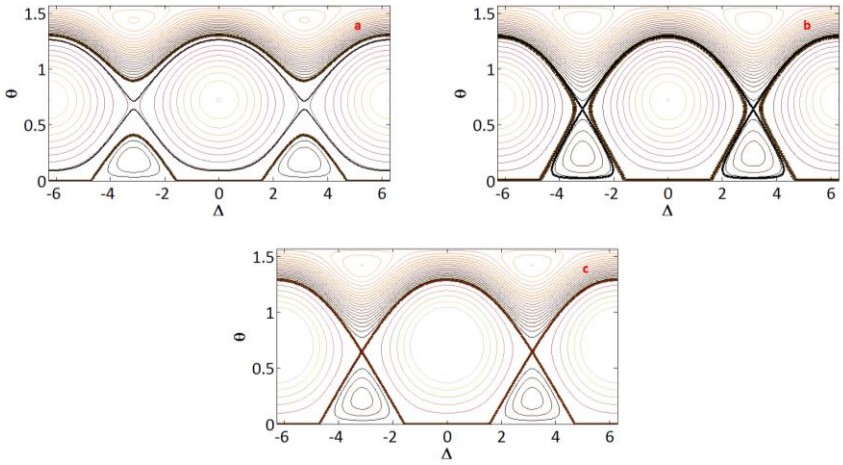

Figure 7. Phase portrait of the reduced system (3.1.20), a) (β=0.15); b) (β=0.18); c) (β=0.1741); The LPT is denoted with a bold solid line.

Surprisingly enough, the derived analytical estimate for the critical coupling strength corresponding to the formation of ELPT-II in the trimer model is fairly close to the true result (i.e. $\beta^1_{LPT} = 0.1741,\ \beta^1_{ELPT} = 0.17101$).

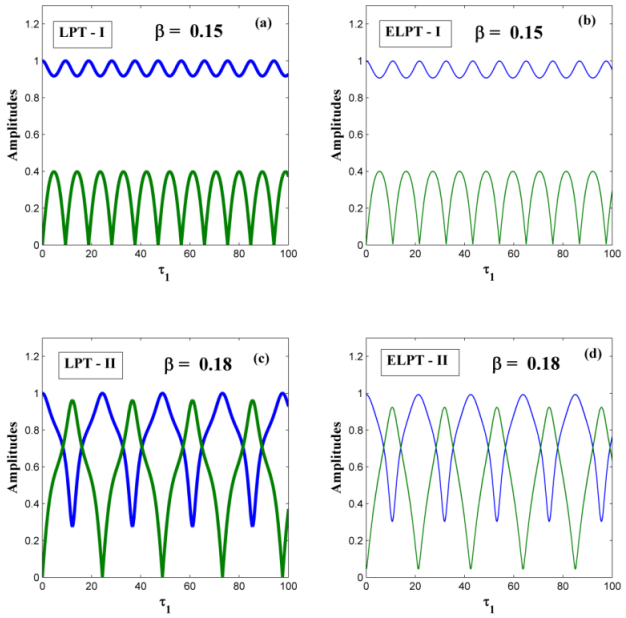

Figure 8. Time histories of LPT of (3.1.20) and ELPT of (3.1.10) (a) (LPT-I) β=0.15; (b) (ELPT-I) β=0.15; (c) (LPT-II) β=0.18; (d) (ELPT-II) β=0.18; LPT is denoted with the bold solid line, ELPT is denoted by. Blue line denotes the amplitude of the response of the first element $\left(\left|\varphi_1(\tau_1)\right|\right)$, the green line denotes the responses of the second one $\left(\left|\varphi_2(\tau_1)\right|\right)$.

3.2.3.2 Analytical estimates of the destruction of ELPT-II

In the previous subsection we observed the second transition (destruction) of ELPT at ($\beta^2_{ELPT} \approx 0.37$). Based on the same 'master-and-slave' decomposition given in (3.1.15) and (3.1.16), we are willing to derive the crude analytical prediction of the destruction of the last surviving, regular transport state manifested by the intense, local energy pulsations.

To find the analytical criterion for the second transition of the ELPT we use the quite naive physical reasoning. In fact as it was discussed in the previous sections, the annihilation of the ELPT-II island is succeeded by the formation of the complete, delocalized resonant energy exchanges among all the elements of the chain. This also means that the third element of the chain becomes strongly excited. This high amplitude excitation of the third element signifies the breakdown of energy localization assumed for the first two elements of the chain resulting in the massive, resonant energy transport to the third element. This spontaneous energy delocalization is a direct outcome of internal resonant excitation of the third element induced by the local resonant pulsations localized on the first two elements of the chain.

This resonance condition can be formulated for the decomposed systems given by (3.1.15) and (3.1.16). As it has been mentioned above, regime of the strongest possible energy pulsations emerging in the first coupled system (3.1.15) exactly corresponds to the LPT of the second kind. This unique solution is used as an external excitation of the second decomposed system (3.1.16). Let us write the response of the second element ($\varphi_2(\tau_1)$) of (3.1.15) corresponding to the limiting phase trajectory of the second kind as,

$$\varphi_{2LPT-II} = \sin\left(\theta_{LPT-II}\right) e^{i\delta_{2LPT-II}} \tag{3.1.26}$$

here $\theta_{LPT-II}, \delta_{2\ LPT-II}$ stand for the angular coordinates of energy distribution and absolute phase accordingly and correspond to the unique limiting phase trajectory of the second kind of the planar system. Using (3.1.26) together with (3.1.16) we focus on the response of the third element given by,

$$\varphi_3{}' = i\beta \sin\left(\theta_{LPT-II}\right) e^{i\delta_{2LPT-II}} \tag{3.1.27}$$

To assess the intrinsic resonance condition between the regime of local energy pulsations (localized on the first two elements of the chain) and the third element we examine the structure of the external force (i.e. $i\beta \sin\left(\theta_{LPT-II}\right) e^{i\delta_{2LPT-II}}$). First of all we notice that the external excitation is composed of the multiplication of the two signals, namely $\sin\left(\theta_{LPT-II}\right)$ and $e^{i\delta_{2LPT-II}}$. Obviously enough, the first signal is perfectly periodic with respect to the fundamental period of the limiting phase trajectory (LPT-II) (i.e. $\sin\left(\theta_{LPT-II}(\tau_1)\right) = \sin\left(\theta_{LPT-II}(\tau_1 + T_{LPT-II})\right)$). Here we denote the period of LPT-II as T_{LPT-II} and the corresponding frequency of energy exchange as $\Omega_{LPT-II} = 2\pi T_{LPT-II}^{-1}$. Theoretical description of the second signal ($e^{i\delta_{2LPT-II}}$) turns out to be a somewhat more complex as the absolute phase ($\delta_2(\tau_1)$) of the second element contains both the monotonously growing component (constant drift) as well as the oscillating one. To show this we reconsider the differential equations depicting the evolution of the absolute phases for the limiting phase trajectory,

$$\begin{aligned}\frac{d\delta_{1LPT}}{d\tau_1} &= \cos^2\left(\theta_{LPT}\right)+\beta-\beta\tan\left(\theta_{LPT}\right)\cos\left(\Delta_{LPT}\right)\equiv f_1\left(\theta_{LPT},\Delta_{LPT}\right)\\ \frac{d\delta_{2LPT}}{d\tau_1} &= \sin^2\left(\theta_{LPT}\right)+2\beta-\beta\cot\left(\theta_{LPT}\right)\cos\left(\Delta_{LPT}\right)\equiv f_2\left(\theta_{LPT},\Delta_{LPT}\right)\end{aligned} \tag{3.1.28}$$

(This set of equations (3.1.28) corresponding to evolution of the absolute phases can be easily derived from (3.1.15) using (3.1.19)). As it was discussed in the previous works [27] θ_{LPT}, Δ_{LPT} are even and odd periodic functions, accordingly, and therefore admit the following cosine and sine Fourier expansions,

$$\theta_{LPT}=A_0+\sum_{n=1}^{\infty}A_n\cos\left(n\Omega_{LPT}\tau_1\right),\ \Delta_{LPT}=\sum_{n=1}^{\infty}B_n\sin\left(n\Omega_{LPT}\tau_1\right) \tag{3.1.29}$$

For the technical reasons pointed out below it is convenient to present the absolute phase of the second element $\delta_2(\tau_1)$ in terms of $\delta_1(\tau_1)$ and Δ_{LPT} functions

$$\delta_{2LPT}=\delta_{1LPT}-\Delta_{LPT} \tag{3.1.30}$$

Using (3.1.29) one can show that the $f_1\left(\theta_{LPT},\Delta_{LPT}\right)$ can be expressed in terms of the Fourier series,

$$f_1\left(\theta_{LPT},\Delta_{LPT}\right)=\Omega_{rot}+\sum_{n=1}^{\infty}\left(D_{1n}\cos\left(n\Omega_{LPT}\tau_1\right)+D_{2n}\sin\left(n\Omega_{LPT}\tau_1\right)\right) \tag{3.1.31}$$

Direct integration of (3.1.31) with respect to τ_1 leads to the following general expression for δ_{1LPT},

$$\begin{aligned}\delta_{1LPT} &= C_0+\Omega_{rot}\tau_1+\sum_{n=1}^{\infty}\left(\tilde{D}_{1n}\cos\left(n\Omega_{LPT}\tau_1\right)+\tilde{D}_{2n}\sin\left(n\Omega_{LPT}\tau_1\right)\right)\\ \tilde{D}_{1n} &= -D_{2n}\left(n\Omega_{LPT}\right)^{-1},\ \tilde{D}_{2n}=D_{1n}\left(n\Omega_{LPT}\right)^{-1}\end{aligned} \tag{3.1.32}$$

Using the Fourier expansion of (3.1.29) and (3.1.32) in (3.1.30), yields, the following general expression for δ_{2LPT},

$$\begin{aligned}\delta_{2LPT} &= C_0+\Omega_{rot}\tau_1+\sum_{n=1}^{\infty}\left(\tilde{D}_{1n}\cos\left(n\Omega_{LPT}\tau_1\right)+\tilde{\tilde{D}}_{2n}\sin\left(n\Omega_{LPT}\tau_1\right)\right),\\ \tilde{\tilde{D}}_{2n} &= \tilde{D}_{2n}-B_n\end{aligned} \tag{3.1.33}$$

Here Ω_{rot} is a special Fourier coefficient corresponding to the rotational speed of the absolute phase. Using, (3.1.26) and (3.1.33) in (3.1.27), yields,

$$\begin{aligned}&\frac{d\varphi_3}{d\tau_1}=\tilde{\beta}\sin\left(A_0+\sum_{n=1}^{\infty}A_n\cos\left(n\Omega_{LPT}\tau_1\right)\right)\exp\left\{i\Omega_{rot}\tau_1\right\}\exp\left\{i\sum_{n=1}^{\infty}\left(\tilde{D}_{1n}\cos\left(n\Omega_{LPT}\tau_1\right)+\tilde{\tilde{D}}_{2n}\sin\left(n\Omega_{LPT}\tau_1\right)\right)\right\}\\ &\tilde{\beta}=i\beta\exp\left\{iC_0\right\}\end{aligned} \tag{3.1.34}$$

As it can be easily inferred from (3.1.34), the secular growth of the response of the third element is obtained when the following (1:1) resonant condition holds,

$$\boxed{\Omega_{LPT}\left(\beta\right)=\Omega_{rot}\left(\beta\right)} \tag{3.1.35}$$

Obviously enough, both Ω_{LPT} and Ω_{rot} depend on the strength of the coupling (β). Thus, finding the explicit dependence of both frequencies (i.e. frequency of the LPT regime and

rotation frequency of the absolute phase) one can roughly estimate the critical value of coupling strength leading to the destruction of the ELPT-II. The details of the approximate analytical solution of (3.1.35) are brought in the appendix. Solution of (3.1.35) yields the critical value of $\beta^2_{ANAL} = 0.3968$.

In addition to the analytic derivation of the theoretical criterion predicting the destruction of ELPT we have used an alternative numerical method based on the Fast Fourier Transform (FFT) illustrating the evolution of both frequencies (i.e. $\Omega_{LPT}, \Omega_{rot}$) with respect to the growing value of the coupling parameter (β) (see **Figure 9**). Both frequencies ($\Omega_{LPT}, \Omega_{rot}$) are extracted from the post-processed, numerically computed signals $Sig1 = \sin(\theta_{LPT-II})$ and $Sig2 = \sin(\delta_{2LPT-II})$. From the diagram of **Figure 9** we find out that the intersection of both the rotation and LPT frequencies (i.e. 1:1 resonance) occurs at $\beta = \beta^2_{ELPT\_FFT} = 0.3649$ which is fairly close to the numerically derived threshold ($\beta = \beta^2_{ELPT} \approx 0.37$). As is also clear from the results of **Figure 9**, the Fast Fourier Transform analysis provides a better prediction than the analytical approximation based on the first order saw-tooth approximation of the limiting phase trajectory. Results of the theoretical predictions and numerical findings (Subsection 3.2.2) of the critical parameters of coupling leading to the formation and the destruction of ELPT-II are summarized in Table 2Error! Reference source not found. and are found to be in the very good agreement with the numerical analysis of the full, slow-flow model (3.1.10).

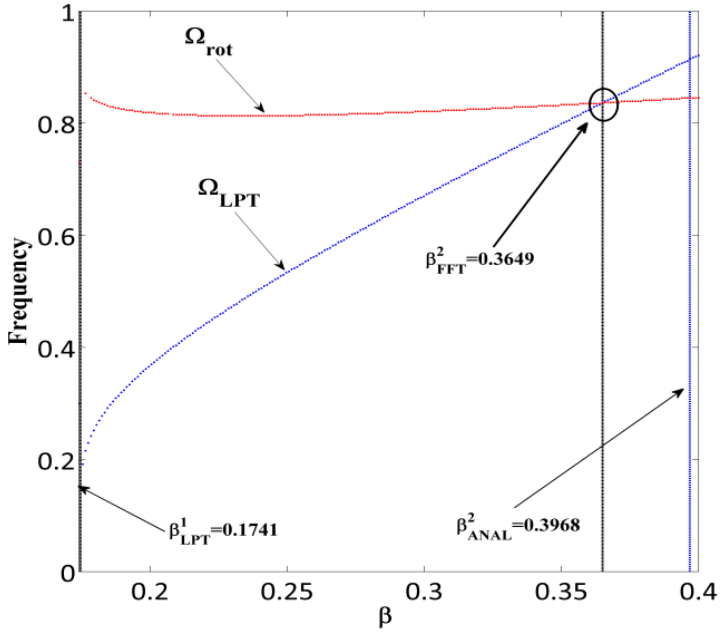

Figure 9. Frequency evolution diagram based on the FFT analysis of (Ω_{LPT} - blue line, Ω_{rot} - red line)

	1st Transition	2nd Transition
ELPT-II Numerical Simulations	$\beta^1_{ELPT} \approx 0.17101$ (Formation of ELPT-II)	$\beta^2_{ELPT} \approx 0.37$ (Destruction of ELPT-II)
ELPT-II Theoretical prediction	$\beta^1_{LPT} = 0.1741$ (Formation of ELPT-II)	$\beta^2_{ANAL} = 0.3968$ (Destruction of ELPT-II) $\beta^2_{FFT} = 0.3649$

Table 2. Transition values for ELPT: Analytical vs. Numerical

4. NUMERICAL SIMULATIONS

4.1. Numerical verifications of the Slow-Flow model

In the present section we perform numerical verifications of the validity of a theoretical model devised in the preceding section. We note that all the numerical integrations of (2.1.1) of the present section have been performed in Matlab using the same ODE45 solver as in Section 3.2.2 with the scalar relative error tolerance of 1×10^{-8} and a vector of absolute error tolerances of 1×10^{-8}. We start numerical verifications from a comparison of the time histories of a true system response (2.1.1) with that of a slow-flow envelope obtained from (3.1.6). To this end we plot the time histories of the response of (2.1.1) corresponding to the case of periodic, energy pulsations predicted by the extended limiting phase trajectories of the slow flow model (3.1.6) (**Figure 10**).

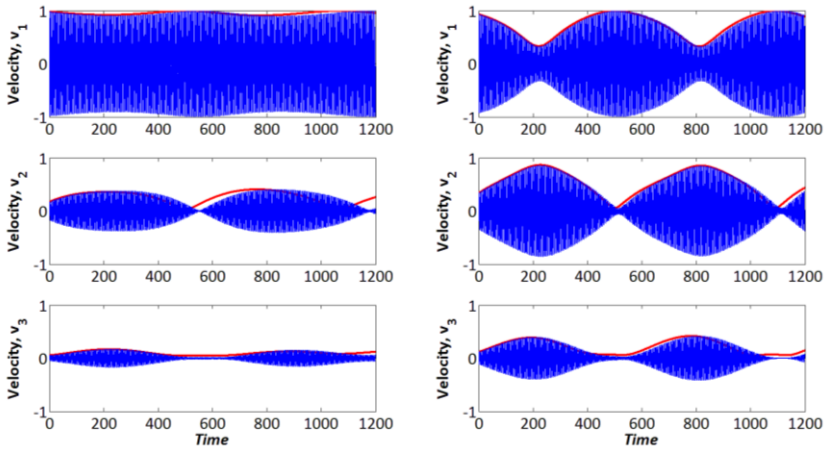

Figure 10. Time histories of the response (velocities) of the original model (2.1.1) vs. slow flow model (3.1.6). (Left panel) Energy localization on the first element corresponding to the ELPT–I, $\beta = 0.15$. (Right panel) Extreme energy transport between the first and the second elements corresponding to the ELPT-II, $\beta = 0.28$.

In **Figure 10** (Left Panel) we plot the response of the full model (2.1.1) predicted by the ELPT-I ($\beta < \beta^1_{ELPT}$) whereas in **Figure 10** (Right Panel) we plot the response of the full model (2.1.1)

predicted by the ELPT-II ($\beta^1_{ELPT} < \beta < \beta^2_{ELPT}$). From the results of **Figure 10** one can clearly observe the very good correspondence between the slow-flow model (2.1.1) and the full model (3.1.6).

4.2 Numerical evidences of the consecutive transitions from localized to delocalized states emerging in the impulsively excited K-G trimer model

To illustrate the importance of the devised theoretical predictive capacity we demonstrate the spontaneous transitions between the different states of energy pulsations emerging in the impulsively excited K-G trimer chain. To this end we perform the series of numerical simulations of the impulsive response (IR) of the full model for the gradually increasing value of the coupling parameter (β). By the term impulsive response we refer to the response of (2.1.1) to the strictly localized initial excitation ($\dot{x}_1(0)=1, x_1(0)=0,\ \dot{x}_i(0)=\dot{x}_i(0)=0,\ (i=2,3)$). The total integration time for each particular run of (2.1.1) is ($T_f = 5000$ time units). For each IR derived from numerical integration of (2.1.1) we compute the maximal amplitude of the instantaneous energy $E_n = \frac{1}{2}\left(\frac{dx_n}{dt}\right)^2 + \frac{1}{2}x_n^2 + \frac{\varepsilon}{4}x_n^4$, ($n=1,2,3$) recorded on each element of the trimer over the entire period of numerical simulation. In **Figure 11** we plot the maximal amplitudes of the response (recorded for each element of the chain) versus the coupling parameter (β).

As is evident from the diagram of **Figure 11** there are two consecutive transitions between the aforementioned pulsating states of the impulsive response. Thus for the lower values of coupling (below the first transition $\beta < \beta_{IR\_I} = 0.1577$) energy is highly localized on the first element of the chain. In this state of the system, weak energy transport from the first element to the rest elements of the chain is recorded. In **Figure 11** this region is labeled as a region of <u>weak energy pulsations</u>.

Right above the first transition threshold ($\beta > \beta_{IR\_I}$) we observe the formation of intense energy pulsations localized between the first two elements of the trimer and low energy excitation recorded on the third one. In **Figure 11** this region of existence of this intermediate state of IR as a region of <u>intense energy pulsations</u>.

Finally, complete delocalization of the IR resulted in the irregular energy pulsations spanning the entire chain can be inferred from the diagram above the second threshold ($\beta > \beta_{IR\_II} = 0.2914$). In this region we specially note the existence of the interior interval ($0.2914 < \beta < 0.3168$) showing the intermittent behavior of the IR. Thus, along with the variation

of the coupling parameter (within this interval) we observe the frequent transitions exhibited by IR between the states of the local intense energy pulsations and complete energy delocalization. In the same diagram (**Figure 11)** we denote this special interval as the region of intermittency. We note that for $0.3168 < \beta$ one can clearly infer from the diagram the elimination of the intermittent behavior of IR followed by the formation of permanent delocalized state. This state is labeled in the diagram (**Figure 11**) as a uniform energy spreading. To showcase the correlation of the spontaneous transitions undergone by IR of (2.1.1) to the evolution of ELPT-II (analyzed in the previous section) we denoted the zone of existence of ELPT-II on the transition diagram (**Figure 11)** with the blue vertical lines**.** As is evident from the results of **Figure 11**, the derived theoretical model provides fairly close though restrictive criteria predicting the zone of existence of the intermediate state of local, intense energy pulsations emerging in the impulsively excited K-G trimer. The critical values of the coupling parameter (β) corresponding to the consecutive transitions of IR of (2.1.1) and these corresponding to the formation and destruction of ELPT-II of (3.1.10) are summarized in Table 3.

5. CONCLUSIONS

In the present work we studied the mechanism of formation and destruction of special class of dynamical regimes manifested by the moderate as well as the intense energy pulsations excited on the first two elements of the anharmonic K-G trimer. Analysis of the global evolution of the slow-flow on the Poincaré maps has revealed the formation of a special type of local, energy-pulsating states corresponding to the periodic and quasi-periodic energy pulsations established between the first two elements of the trimer. As it is shown in the paper this special locally pulsating, periodic regime constitute the higher dimensional analog of the limiting phase trajectory considered in the 2DOF anharmonic, non-symmetric models and is referred to as ELPT. Detailed analytical and numerical study of the formation and destruction of this special dynamical regime is pursued in the paper. We show that unlike its lower dimensional counterpart, extended limiting phase trajectory undergoes additional bifurcation leading to its complete elimination. The mechanism of formation and destruction of this special dynamical state is predicted using the reduced order model.

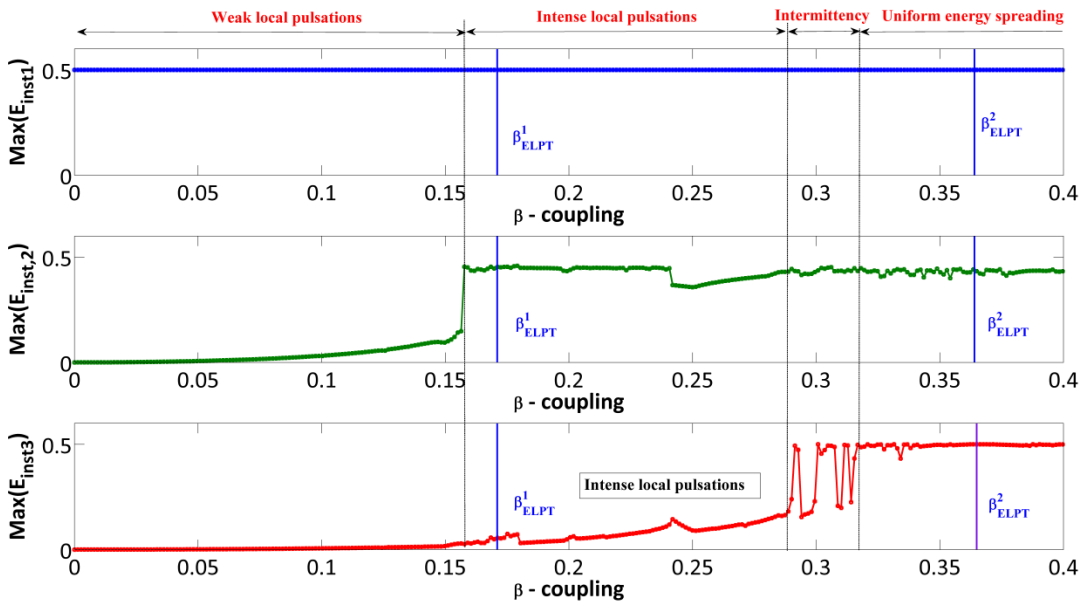

Figure 11. Consecutive transitions of the IR from the highly localized to delocalized transport state in the original model (2.1.1). **Upper panel**: the first element, **Central panel**: the central element, **Lower panel**: the third element. The first and the second transitions undergone by the IR and the ELPT-II obtained in the slow-flow model (Table 3) are marked with the vertical, solid lines, accordingly. Initial conditions: $x_k(0)=0,\ x_k'(0)=\delta_{1k},\ k=1,2,3$.

Using the previous results of the limiting phase trajectories we predict analytically the two consecutive transitions undergone by the ELPT. As it is confirmed by the numerical simulations of both slow-flow and the full models, the formation and destruction of the ELPT-II provides the rather restrictive criteria for the zone of existence, of the special dynamical states of intense energy pulsations - localized on the first two elements of the impulsively excited K-G trimer. All the analytical results are in a good agreement with numerical simulations of both slow-flow model and the original system.

	1st Transition	**2nd Transition**
Impulsive response of the K-G trimer (Full-Model (2.1.1))	$\beta_{IR}^{1} \approx 0.1577$	$\beta_{IR}^{2} \approx 0.2914$
ELPT-II Poincaré maps (**Slow-Flow**)	$\beta_{ELPT}^{1} \approx 0.17101$ (Formation of ELPT-II)	$\beta_{ELPT}^{2} \approx 0.37$ (Destruction of ELPT-II)
ELPT-II- Theoretical prediction **(Slow -Flow)**	$\beta_{ANAL}^{1} = 0.1741$ (Formation of ELPT-II)	$\beta_{FFT}^{2} = 0.3649$ $\beta_{ANAL}^{2} = 0.3968$ (Destruction of ELPT-II)

Table 3. Summary of the transition values for the IR of the full (2.1.1) and slow-flow models (3.1.7).

APPENDIX

As it was demonstrated in the previous studies the limiting phase trajectory of the second kind can be approximated by employing the method of non-smooth time transformations (NSTT) developed at first by Pilipchuck [39-41]. Thus, recent works [19-29] devoted to the analysis of LPTs in the lower dimensional systems, have shown that the waveform of these trajectories can be approximated in terms of the saw-tooth functions.

$$\tau = \frac{2}{\pi}\left|\arcsin\left(\sin\left(\frac{\pi t}{2}\right)\right)\right|,\ e = \frac{d\tau}{dt} \tag{A.1}$$

It is rather natural to seek for the LPT solution using the basis of saw-tooth functions (A.1), in the following form,

$$\theta = X_\theta(\tau) + eY_\theta(\tau); \delta = X_\delta(\tau) + eY_\delta(\tau), \tau = \tau\left(\tau_1 \big/ a\right) \tag{A.2}$$

Using simple algebraic manipulation it can be easily shown that $Y_\theta(\tau) = X_\delta(\tau) = 0$. Substituting (A.2) into (3.1.20), yields

$$\begin{aligned} &X_\theta{}' = a\beta \sin Y_\delta \\ &\sin(2X_\theta)Y_\delta{}' = \frac{a}{2}\sin(4X_\theta) + 2a\beta\cos(2X_\theta)\cos(Y_\delta) - a\beta\sin(2X_\theta) \\ &Y_\delta(\tau)|_{\tau=1} = 0 \end{aligned} \tag{A.3}$$

where $(.)'$ stands for the first derivative with respect to the non-smooth function (τ). Proceeding with the method of successive approximations we assume the following generating function for the angular variable θ_{LPT} at the first stage of approximation,

$$X_\theta^{(1)} = K\tau\left(\tau_1 \big/ a\right), Y_\delta^{(0)} = \begin{cases} 0, & \tau \neq 1 \\ K, & otherwise \end{cases} \tag{A.4}$$

Plugging (A.4) into the first equation of (A.3), yields

$$X_\theta^{(1)\prime} = a\beta \sin K \tag{A.5}$$

Solution of (A.5) reads,

$$X_\theta^{(1)} = (a\beta \sin K)\tau\left(\tau_1 \big/ a\right) \tag{A.6}$$

Consistency relation between (A.6) and the first equation of (A.4), yields the important relation between the period of energy exchange process ($2a$) and the amplitude of the limiting phase trajectory (K)

$$T_{LPT} = 2a = \frac{2K}{\beta \sin K}\ ,\ \Omega_{LPT} = 2\pi\left(T_{LPT}\right)^{-1} = \frac{\pi\beta \sin K}{K} \tag{A.7}$$

To find the approximation for the amplitude of the limiting phase trajectory (K) we resort to the corresponding Hamiltonian of the planar system (3.1.24). Thus plugging (A.2) into (3.1.24), yields

$$\sin^2\left(2X_\theta(\tau)\right) + 4\beta\sin\left(2X_\theta(\tau)\right)\cos\left(e(\tau)Y_\delta(\tau)\right) - 4\beta\sin^2\left(X_\theta(\tau)\right) = 0 \tag{A.8}$$

Inserting the obtained approximation (A.4) into (A.8) and imposing the boundary conditions defined in (A.3) ($Y_\delta(\tau)|_{\tau=1}=0$), yields

$$\sin^2(2K)+4\beta\sin(2K)-4\beta\sin^2(K)=0 \qquad \text{(A.9)}$$

Equation (A.9) implicitly defines the amplitude of LPT as a function of coupling parameter ($K=K(\beta)$). Thus, solving (A.7) and (A.9) simultaneously for the given value of coupling (β) yields the time period (T_{LPT}) and consequently the frequency ($\Omega_{LPT}=2\pi(T_{LPT})^{-1}$) of the limiting phase trajectory (LPT) of the second kind. It is worth noting that the equation (A.8) can be used further for the derivation of the next order approximation for the $Y_\delta(\tau)$

$$Y_\delta^{(1)}=\cos^{-1}\left[\frac{1}{2}\left\{\tan\left(X_\theta^{(1)}\right)-\beta^{-1}\sin\left(X_\theta^{(1)}\right)\cos\left(X_\theta^{(1)}\right)\right\}\right],\ \tau\neq 1 \qquad \text{(A.10)}$$

In **Figure A1** (a, b) we plot the time histories of the response of the planar system (3.1.20) corresponding to the limiting phase trajectory together with its first order approximation.

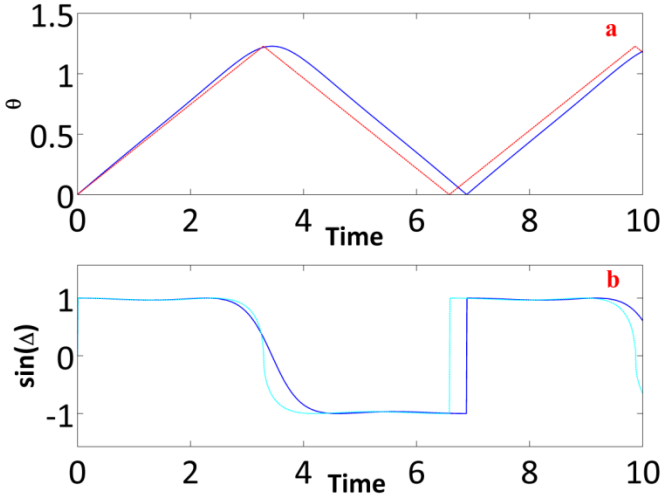

Figure A1. Time histories of the response of the planar system (3.1.20) corresponding to the limiting phase trajectory. Numerical simulation of (3.1.20) is denoted with the solid blue lines, analytical approximation is denoted with the solid red and light blue lines

Our next goal is finding the analytical approximation for the rotation frequency of the absolute phase (Ω_{rot}) defined above. According to (3.1.31) Ω_{rot} is the first Fourier coefficient in the expansion which is defined as follows,

$$\Omega_{rot}=\frac{1}{T_{LPT}}\int_0^{T_{LPT}} f_1\left(\theta_{LPT}(\tau_1),\Delta_{LPT}(\tau_1)\right)d\tau_1 \qquad \text{(A.11)}$$

Using the derived approximation ($\theta_{LPT}=X_\theta^{(1)},\Delta_{LPT}=Y_\theta^{(1)}e$) in (3.3.35) one arrives at the following closed form approximation corresponding to the rotation frequency of the absolute phase,

$$\Omega_{rot}=\frac{3}{2}\beta+\frac{3}{4}+\frac{\sin(2K)}{8K}-\beta\frac{\tan(K)}{2K} \qquad \text{(A.12)}$$

Equating Ω_{LPT} (given in (A.7)) with (A.3) and accounting for (A.9) we obtain the theoretical prediction for the critical value of the coupling parameter ($\beta^2_{ELPT\_ANAL} = 0.3968$) corresponding to the destruction of the entire state of local, intense energy transfer. This case of the destruction of the resonance islands corresponding to (ELPT-II) has been observed in the Poincaré section of **Figure 4**.

ACKNOWLEDGMENTS

The authors are grateful to Israel Science Foundation (Grant No. 484 /12) and German Israeli Foundation (Grant No. 2017895) for financial support.

REFERENCES

[1] A. F. Vakakis, O. Gendelman, L. A. Bergman, D. M. McFarland, G. Kerschen, and Y. S. Lee, Passive Nonlinear Targeted Energy Transfer in Mechanical and Structural Systems Springer-Verlag, New York, (2008)

[2] K. Hasselmann. On the non-linear energy transfer in a gravity-wave spectrum. I. General theory. J. Fluid Mech., 12:481–500, 1962.

[3] D. J. Benney and P. Saffman. Nonlinear interaction of random waves in a dispersive medium. Proc. Roy. Soc. London, 289(1418):301–320, January 25 1966.

[4] J. Benney and A. C. Newell. Random wave closure. Stud. in Appl. Math., 48:1, 1969.

[5] Alan C. Newell. Wave turbulence is almost always intermittent at either small or large scales. Stud. Appl. Math., 108(1):39–64, 2002.

[6] Alan C. Newell, Sergey Nazarenko, and Laura Biven. Wave turbulence and intermittency. Phys. D, 152/153:520–550, 2001. Advances in nonlinear mathematics and science.

[7] B. B. Kadomtsev. Plasma turbulence. Academic Press, New York, 1965.

[8] Yuri V. Lvov and Esteban G. Tabak. Hamiltonian formalism and the Garrett-Munk spectrum of internal waves in the ocean. Phys. Rev. Lett., 87(16):168501, October 15 2001.

[9] Y. V. Lvov, R. Binder, and A. C. Newell. Quantum weak turbulence with applications to semiconductor lasers. Physica D, 121:317–343, 1998.

[10] Y. V. Lvov and A. C. Newell, Phys. Rev. Lett. 84, 1894, 2000.

[11] Y. V. Lvov and A. C. Newell, Phys. Lett. A 235, 499, 1997.

[12] G. Kopidakis, S. Aubry, and G. P. Tsironis, Targeted Energy Transfer through Discrete Breathers in Nonlinear Systems, Phys. Rev. Lett. 87, (2001), 165501

[13] S. Aubry, G. Kopidakis, A. M. Morgante, and G. P. Tsironis, Physica B 296, 222 (2001).

[14] P. Maniadis, G. Kopidakis, and S. Aubry, Physica D 188, 153 (2004).

[15] P. Maniadis and S. Aubry, Physica D 202, 200 (2005).

[16] Localization and Energy Transfer in Nonlinear Systems, edited by L. Vazquez, R. MacKay, and M. P. Zorzano (World Scientific, Singapore, 2003).

[17] Energy Localization and Transfer, edited by T. Dauxois, A. Litvak-Hinenzon, R. MacKay, and A. Spanoudaki (World Scientific, Singapore, 2004).

[18] A. F. Vakakis, L.I. Manevitch, Yu.V. Mikhlin, V.N. Pilipchuk, A.A. Zevin, Normal Modes and Localization in Nonlinear Systems, Wiley, New York, 1996.

[19] L. I. Manevitch, Arch. Appl. Mech. 77, 301 (2007)

[20] L.I. Manevitch, A. Kovaleva, E.L. Manevitch, D.S. Shepelev, Limiting phase trajectories and non-stationary resonance oscillations of the Duffing oscillator, Part 1. A non-dissipative oscillator, Commun. Nonlinear Sci. Numer. Simulat., 16 (2011) 1089-1097.

[21] L.I. Manevitch, A. Kovaleva, E.L. Manevitch, D.S. Shepelev, Limiting phase trajectories and non-stationary resonance oscillations of the Duffing oscillator. Part 2. A dissipative oscillator, Commun. Nonlinear Sci. Numer. Simulat. 16 (2011) 1098-1105.
[22] L.I. Manevitch, A. Kovaleva, D.S. Shepelev, Non-smooth approximations of the limiting phase trajectories for the Duffing oscillator near 1:1 resonance. Physica D 240 (2011) 1-12.
[23] Y. Starosvetsky, L.I. Manevitch, Nonstationary regimes in a Duffing oscillator subject to biharmonic forcing near a primary resonance, Phys. Rev. E 83 (2011) 046211 (1-14).
[24] L.I. Manevitch, M.A. Kovaleva, V.N. Pilipchuk, Non-conventional synchronization of weakly coupled active oscillators, Europh. Lett. 101 (2013) 50002 (1-5).
[25] L.I. Manevitch, A.I. Musienko, Limiting phase trajectories and energy exchange between anharmonic oscillator and external force, Nonlinear Dynamics 58 (2009) 633-642.
[26] L.I. Manevitch, A. Kovaleva, Nonlinear energy transfer in classical and quantum systems, Phys. Rev. E 87 (2013) 022904 (1-12).
[27] L.I. Manevitch, O. Gendelman, Tractable Models of Solid Mechanics, Springer-Verlag, Berlin, Heidelberg, 2011.
[28] Y. Starosvetsky, Y. Ben-Meir, Nonstationary regimes of homogeneous Hamiltonian systems in the state of sonic vacuum, Phys. Rev. E 87 (2013) 062919 (1-18)
[29] A. Kovaleva, L.I. Manevitch, E.L. Manevitch, Intense energy transfer and superharmonic resonance in a system of two coupled oscillators, Phys. Rev. E 81 (2010) 056215 (1-12).
[30] L.I. Manevitch, V.V. Smirnov. Localized nonlinear excitations and interchain energy exchange in the case of weak coupling, in: Jan Awrejcewicz (Ed.). Modeling, Simulation and Control of Nonlinear Engineering Dynamical System, Springer Netherlands, 2009, pp.37-47.
[31] L.I. Manevitch, V.V. Smirnov, Limiting phase trajectories and the origin of energy localization in nonlinear oscillatory chains, Phys. Rev. E 82 (2010) 036602 (1-9).
[32] L.I. Manevitch, V.V. Smirnov, Resonant energy exchange in nonlinear oscillatory chains and Limiting Phase Trajectories: from small to large systems, in: A.F. Vakakis (Ed.), Advanced Nonlinear Strategies for Vibration Mitigation and System Identification, CISM Courses and Lectures, 518, Springer Wien New York, 2010, pp. 207-258.
[33] A. Kovaleva, L.I. Manevitch, Classical analog of quasilinear Landau-Zener tunneling. Phys. Rev. E, 85 (2012) 016202 (1-8).
[34] A. Kovaleva, L.I. Manevitch, Limiting phase trajectories and emergence of autoresonance in nonlinear oscillators, Phys. Rev. E 88 (2013) 024901 (1-6).
[35] A. Kovaleva, L.I. Manevitch, Yu.A. Kosevich, Fresnel integrals and irreversible energy transfer in an oscillatory system with time-dependent parameters, Phys. Rev. E 83 (2011) 026602 (1-12).
[36] J. De Luca, A.J. Lichtenberg, M.A. Lieberman, Time scale to ergodicity in the Fermi-Pasta-Ulam system
[37] A. J. Lichtenberg, R. Livi, M. Pettini, S. Ruffo, Dynamics of Oscillator Chains, Lecture Notes in Physics, The Fermi-Pasta-Ulam Problem (A status report), Springer-Verlag Berlin Heidelberg (2008) DOI: 10.1007/978-3-540-72995-2
[38] G. Sigalov, L. Manevitch, F. Romeo, L. A. Bergman, A. F. Vakakis, Dynamics of a linear oscillator coupled to a bistable light attachment: analytical study, J. Appl. Mech. (2013) doi:10.1115/1.4025150.
[39] Pilipchuk V. N., Nonlinear Dynamics: Between Linear and Impact Limits (Springer, New York) 2010.
[40] Pilipchuk V. N., Oscillators with a generalized power-form elastic term, Journal of sound and vibration (2004), 270 (1), 470-472
[41] Pilipchuk V. N., ANALYTICAL STUDY OF VIBRATING SYSTEMS WITH STRONG NON-LINEARITIES BY EMPLOYING SAW-TOOTH TIME TRANSFORMATIONS, Journal of Sound and Vibration (1996) 192(1), 43–64